Morphology of $TiSi_2$ and $ZrSi_2$ on Si(100) and (111) surfaces

C. A. Sukow and R. J. Nemanich
Department of Physics and Department of Materials Science and Engineering, North Carolina State University, Raleigh, North Carolina 27695-8202

(Received 2 August 1993; accepted 12 January 1994)

The morphologies of $ZrSi_2$ on Si(111) and $TiSi_2$ on Si(111) and (100) have been investigated, and the results compared and contrasted. Films were prepared by UHV deposition of Ti or Zr onto clean, reconstructed Si(100) or (111) substrates, and reacted by *in situ* annealing. The sheet resistivity of the $ZrSi_2$ was measured and found to be 33–42 $\mu\Omega$-cm. The morphologies were examined by transmission and scanning electron microscopy. In particular, the islanding properties were studied; both the temperature of the onset of islanding and the island characteristics were measured. The surface and interface energies have been determined from the contact angles of the silicide islands, according to a solid-state capillarity model. The system of $ZrSi_2$ on Si(111) was found to have surface and interface energies lower than those of the system of $TiSi_2$ on Si(100), but higher than those of the system $TiSi_2$ on Si(111). $ZrSi_2$ on Si(111) was found to island at a higher temperature than $TiSi_2$ on either substrate, a result attributed to kinetic effects. Areal coverage of the islands was measured, and the results were consistent with the solid-state capillarity model. For both $TiSi_2$ and $ZrSi_2$, increasing faceted structure was observed with increasing anneal temperature. Preferred faceting planes were found to be of Si(111) and (100) type for $TiSi_2$ islands and of Si(111) type for $ZrSi_2$. Faceted islands were apparently epitaxial. As the solid-state capillarity model does not directly apply to islands with a faceted structure, an observation of the percentage of faceted islands produced by different annealing temperatures was used to suggest the processing conditions in which the model is applicable.

I. INTRODUCTION

The need for new materials to be used as contacts and interconnections in microelectronic devices has been apparent in the face of ever-decreasing device dimensions. For interconnects, the doped polysilicon lines often used, while having several other favorable properties, have too high a resistance (~500 $\mu\Omega$-cm) to be useful for some VLSI applications. Many different metal silicides, among them Ti, Ta, W, Mo, and more recently Zr, with resistivities an order of magnitude less than polysilicon, have been studied as possible interconnect materials.[1] To limit reactions with underlying structures, these silicides have been used as shunts over polysilicon. These "polycides" thus capitalize on both the good interface qualities of the polysilicon and the low resistivity of the silicide. The same silicides are often considered for source or drain contacts. In these applications, the metal is deposited directly onto the crystalline substrate and annealed to cause a thin film reaction.

Titanium silicide has long been of interest for use in contacts and interconnects on VLSI devices, because it exhibits the lowest resistivity of the common refractory silicides. The material has a major drawback, however, in that it shows a persistent tendency for surface roughening or islanding. Previous studies have examined this islanding problem in relation to the surface and interface energies of titanium silicide on the (111) and (100) faces of silicon.[2] This study will enlarge upon that approach by introducing a comparison with a system in which both the film and the substrate are varied. Zirconium silicide on silicon is the system chosen, largely because of its similarity to the $TiSi_2$/Si system. The purpose of this work is twofold: to use a study of the $ZrSi_2$/Si system to better understand the $TiSi_2$/Si system; and in a preliminary way to explore the potential of the $ZrSi_2$/Si system.

The main comparison that will be made between the two systems is that of the surface and interface energies. A key aspect of the comparison is that both material systems exhibit the same crystal structure, namely the C49 structure. In this study, contact angle measurements are obtained from TEM measurements and analyzed in terms of a solid-state capillarity model, to determine the film surface and interface energies. Other than prior similar measurements,[2] we are not aware of other measurements or estimates of the surface energies of either silicide. These measurements are then used to gain insight into the forces driving the silicide morphologies. Prior studies have been preliminary values of the surface and interface energies of $TiSi_2$ on Si(111) and (100).[3] This study refines some of those results and also includes measurements of the surface and interface energies of

 © 1994 Materials Research Society

the $ZrSi_2$/Si(111) system. In this way, the surface and interface energies of the chemically similar $TiSi_2$ and $ZrSi_2$ films can be varied, whereas in the prior work the emphasis was on the variation of the substrate surface energy [i.e., Si(100) vs Si(111) surfaces].

A wide range of the properties of silicides have been addressed in a review by Murarka.[1] Here, and elsewhere, we find more than adequate justification for the consideration of $ZrSi_2$. The material has multiple chemical and physical similarities to the $TiSi_2$ system. The valence electronic structures of Zr and Ti are the same (both are column 4 transition metals). The orthorhombic C49 structure is shared by $ZrSi_2$ (a = 3.698 Å, b = 14.761 Å, and c = 3.664 Å)[4] and the metastable phase of $TiSi_2$. $ZrSi_2$ is stable in the C49 structure, while C49 $TiSi_2$ (a = 3.62 Å, b = 13.76 Å, and c = 3.60 Å)[5] undergoes a phase transition to the C54 structure (a = 8.2682 Å, b = 4.8001 Å, and c = 8.5531 Å)[4] when annealed to higher temperatures (650 °C–800 °C, depending on film thickness and experimental conditions). The sheet resistivity of the $ZrSi_2$ films grown for this study was measured to be 33–42 $\mu\Omega$-cm, a value approaching that of the low-resistivity C54 phase of $TiSi_2$ (13–25 $\mu\Omega$-cm). Other investigators[6,7] have found similar values for the resistivity of $ZrSi_2$. The Schottky barrier heights of the two silicides are comparable ($ZrSi_2$, 0.55 eV; $TiSi_2$, 0.6 eV, both on n-type Si); both are useful for contact applications on either p- or n-type silicon, considering that a relatively low Schottky barrier is preferred for ohmic contacts. The melting points are high ($ZrSi_2$, 1650–1700 °C; $TiSi_2$, 1540 °C), indicating that $ZrSi_2$ is as suitable for high-temperature processing as $TiSi_2$. $ZrSi_2$ also shares with $TiSi_2$ favorable characteristics, such as stability in oxidizing conditions and a low volume change for the silicide formation.[1] It has been reported, however, that while $TiSi_2$ shows very little anisotropy in the expansion of the a-, b-, and c-axes, the a-axis of $ZrSi_2$ expands ~60% more than the b-axis.[4]

The reaction sequences and the products formed by use of various growth and reaction parameters have been the subject of several studies. The bulk of the evidence[2,8–12] indicates that for the reactions of the Ti–Si system, the sequence for reaction of a Ti film on a Si substrate is as follows: intermixing of the Ti and Si at temperatures of 200–450 °C, at which point the C49 phase of $TiSi_2$ nucleates. The stable C54 phase of $TiSi_2$ forms at temperatures ranging from 650 to 800 °C. While the temperature of the C49 to C54 transition for thin film couples has been shown to depend on extrinsic factors such as grain size[13] and impurity content, it was shown that the C49 to C54 transition was dependent on deposited Ti thickness.[2] Substantially higher temperatures are required for films less than 400 Å thick. In fact, for silicides formed with less than 100 Å Ti on Si(111), the C49 phase was stable to temperatures >900 °C, and for 100 Å Ti on Si(100) the transition was between 700 and 800 °C. In the studies described here, contact angle measurements were obtained from films deposited in UHV with Ti thickness ≤100 Å. Thus, the $TiSi_2$ exhibits the C49 phase in all cases except 800 °C and 900 °C anneals on Si(100).

The reaction sequence of Zr and Si exhibits some differences from that of Ti on Si. Previous studies of the reaction sequence of the Zr–Si system have indicated that an amorphous Zr–Si interlayer initially forms at ~420 °C.[14–17] Formation of ZrSi is the initial crystalline silicide. Annealing to ≥650 °C results in the formation of C49 $ZrSi_2$ phase. This is apparently the final and stable phase in contact with the Si substrate. Several workers have reported the growth of epitaxial films, which may be desirable because the effects of epitaxy can increase film stability and decrease resistivity. A table of the reported epitaxial relations has been compiled elsewhere.[18]

Since it is important, in order that these materials behave predictably and reliably in devices, that the films be smooth and uniform, film morphology has also been a topic of interest. Several workers[2,19–21] have reported that $TiSi_2$ films degrade (that is, change from uniform coverage to an island morphology) with heat treatment; this effect will also be addressed in this work. Omura *et al.*[22] have found that a Ti-ion implantation method produces smoother films than the sputter deposition method, Kuwano *et al.*[23] have produced similar improvements by the use of Xe^+-implanted polysilicon substrates, and Chen *et al.*[24] have also found backsputter cleaning to be of use to this end. Revesz *et al.*[19] have proposed a model for the mechanism of island formation, indicating a process of solution and transport of Si atoms in $TiSi_2$, followed by the precipitation and epitaxial regrowth of Si, which deforms the neighboring $TiSi_2$ into islands. Therefore, agents that inhibit Si mobility (such as impurities, as noted above) improve the film morphology. Interface morphology has been studied by Catana and co-workers,[25,26] and in earlier work in our laboratory.[2,3] Various interface structures have been observed on a near-atomic scale, some quite flat and others faceted. It is important to note that different structures may be present on a single island, so that on the scale of the island the apparent morphology is often a combination of structural effects.

Less has been reported regarding the morphology of $ZrSi_2$ films. In most of the studies that show plan-view type data, the films appear to be polycrystalline and of high areal coverage (see, for example, Mu *et al.*[27] and this work). Bourret and co-workers[28] have presented an analysis of polytypes which appear in $ZrSi_2$ thin films, information also applicable to C49 $TiSi_2$. They find a

$\pi/2$-rotation twin around the b-axis, occurring in the (010) plane, with an average distance between faults of 1.6 nm. A strained lattice, with an averaged $a = c$ lattice parameter, results from the fact that an equal number of $\langle a \rangle$- and $\langle c \rangle$-oriented slabs occur.

Attempts to explain the phenomena associated with silicides and their formation have involved both kinetics and energetics. An earlier paper by Botha and Pretorius[29] used a radioactive Si marker to determine the diffusing species in the formation of different silicides, and found that in both $TiSi_2$ and $ZrSi_2$ the diffusing species is Si. The mechanism of diffusion was found in both silicides to be silicon substitutional (vacancy) diffusion. In previous studies, it was proposed that surface and interface energies play a role in both the nucleation and phase formation of the silicides.[2,30,31] For $TiSi_2$, it was proposed that the lower surface and interface energies of the C49 phase resulted in a lower nucleation barrier than the C54 $TiSi_2$ phase.

The formation of island structures is also strongly dependent on surface and interface energies. An island formation process based on energy considerations has been presented by Nolan *et al.*[32] Their "grain boundary grooving" model postulates that the driving force for surface roughening (i.e., the formation of islands) is the equilibrium among the surface energy of the film, the interface energy of the grain boundary, and the interface energy between the film and substrate. They calculate a minimum grain size, for any given initial thickness, below which the surface roughening is not energetically favored to occur. Some of the predictions made in that study were limited by the fact that values for the surface and interface energies of silicides were not available. d'Heurle also presents an extensive study of the energy considerations involved in nucleating a new phase AB from two phases, A and B, which are in contact with each other.[33] The "geometric considerations" discussed in that study are closely related to the model to be used in this work. Energy considerations are also used in the interpretation of experimental results in studies by van Houtum *et al.*,[13] Chu *et al.*,[34] and in previous work in our laboratory.[2,3]

This paper will employ a solid-state capillarity model, some aspects of which have been presented earlier.[2] With this model, values of the surface and interface energies of $TiSi_2$ and $ZrSi_2$ on silicon substrates will be determined, and morphological observations will be correlated to predictions of the model. The model itself will be discussed in some detail. The energy requirements for the elimination of islanding, and potential methods for satisfying those requirements, will also be addressed in this work. The limits of the applicability of the model will also be considered. Specifically, we make observations regarding the annealing conditions required to produce islanding, the appearance of faceted islands, and measurement of the areal coverage of the islands. We shall give special attention to one type of morphology that is not addressed by the model, namely, the appearance of faceted islands.

II. SOLID STATE CAPILLARITY MODEL

The basis of the solid-state capillarity model is the well-established study of the surface and interface energies of liquids. For the model as applied here, the surface energies of the film and substrate and the interface energies are involved in determining the morphology. It is the balancing of these three energies (surface energy of substrate, surface energy of film, and interface energy) that the solid-state capillarity model focuses on in attempting to explain the observed morphologies.

The essential features of the solid-state capillarity model are given below; other aspects, not needed here, have been presented elsewhere.[2] First, it is assumed that during annealing, when the disilicide is being formed, the disilicide and the silicon substrate behave as immiscible liquids, and this character is reflected in their post-annealing appearance as well. Of course, the temperatures to which the wafers are annealed are below the melting temperatures of the materials used, so the system is never liquid. Second, the island formation process is assumed to be driven by energetics rather than being limited by kinetics (diffusion), as sufficient thermal energy is supplied during the anneal to allow interdiffusion of the silicon and the metallic thin film. Third, the islands are assumed to have reached an equilibrium state, in which the shape of the islands is determined by an equilibrium configuration of the surface free energies of the film and the substrate, and the free energy of the interface between them. If the surface energy of the substrate is known, then, by measuring the angles formed by the two surfaces and the interface, with the point of contact as the vertex of all three angles, the energies of the film and the interface may be deduced by the direct application of the theorem of Neumann's triangle. The angles and surface energy vectors are defined in Fig. 1.[35] For this situation, the relation between the energies and angles is given by the following expression:

$$\frac{\sigma_{\text{film}}}{\sin \theta_{\text{film}}} = \frac{\sigma_{\text{interface}}}{\sin \theta_{\text{interface}}} = \frac{\sigma_{\text{Si}}}{\sin \theta_{\text{Si}}}, \qquad (1)$$

where σ_{film}, σ_{Si}, and $\sigma_{\text{interface}}$ are the film surface energy, the Si surface energy, and the interface energy, respectively, and θ_{film}, θ_{Si}, and $\theta_{\text{interface}}$ are the contact angles as indicated in Fig. 1.

The surface and interface energies often determine whether the film will form islands or wet the surface of the substrate. In general, the surface(s) with higher energy will be minimized, affecting a number of morphological characteristics such as areal coverage and degree

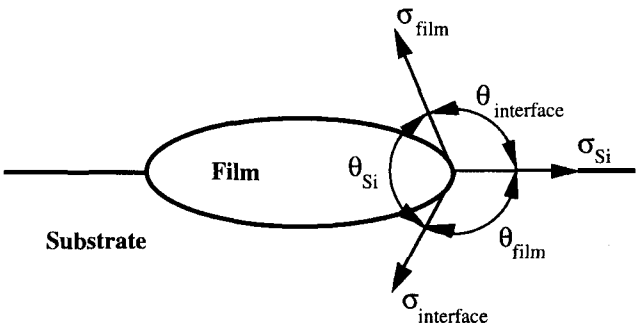

FIG. 1. A schematic cross section of an island on a substrate. The surface and interface energy vectors and corresponding contact angles are shown for the island within the solid-state capillarity model analysis.

of recession of the island into the substrate. The relation of film morphology and surface and interface energies are shown schematically in Fig. 2. The equilibrium condition in which an island rests upon the substrate without spreading occurs when none of the energies are greater than the sum of the other two. If one of these conditions is not met, the resultant film morphology is expected to be either uniform coverage or agglomeration either above or below the surface of the substrate, as illustrated in Fig. 2.

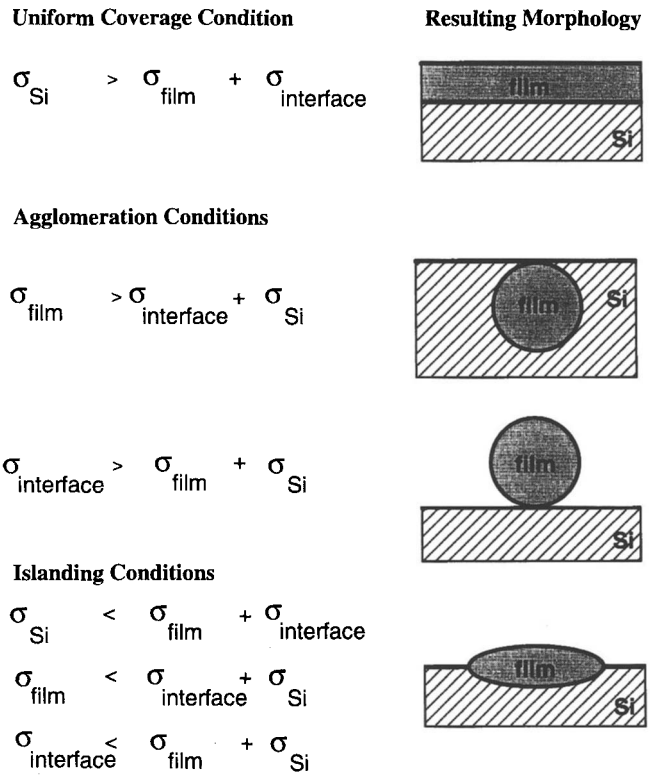

FIG. 2. Limiting conditions for various morphologies within the solid-state capillarity model.

The minimum condition for a uniform coverage is also a "limiting condition" for islanding, and for the silicide/Si system would be given by

$$\sigma_{Si} = \sigma_{film} = \sigma_{interface} \quad (2)$$

This model is, of course, idealized and neglects other influences on the formation and morphology of the disilicide islands, such as interface bonding, strain, and kinetic effects. The effect of interface bonding could result in a preferred crystallographic plane, which would likely cause stabilization of the island in a particular orientation with respect to the substrate. This effect is essentially the same as epitaxial growth, since an island with a specific crystallographic orientation with respect to the substrate is one definition of epitaxy. When a preferred alignment occurs, the interface morphology of the island would reflect the existence of the lower-energy plane by displaying an extended region of flat interface. If multiple possible preferred planes exist, the island may take on a faceted appearance.

The effects of kinetic, or diffusion, limitations on island formation and morphology can be subtle. In a system where such limitations were extreme, they would probably be manifested by an inability to form even a completely reacted film in reasonable times. Since that is obviously not the case in the systems and conditions under consideration, we expect that the effects of kinetic limitations are minor in comparison with the energetic driving forces. However, the degree of diffusion limitation will in general be different for different materials, thus complicating the interpretations of results in comparative studies.

III. EXPERIMENTAL

Silicon (111) and (100) wafers (*n*-type, *P*-doped, resistivity 0.8–1.2 Ω-cm, 25 mm diameter) to be used for substrates were cleaned first by uv-ozone and then by an HF spin etch. The spin etch used HF-H_2O-ethanol at 1:1:10. Within the space of minutes, the wafer was transferred to the turbo-pumped load lock chamber. After evacuation to $<1 \times 10^{-6}$ Torr in ~30 min, the wafer was transferred to the UHV deposition chamber. Before deposition, the wafer was subjected to an 850 °C, 10–15 min heat clean in UHV, which produced reconstructed surfaces: 2×1 on the (100) wafers and 7×7 on the (111) wafers. A resistively heated tungsten filament, positioned ~2 mm from the back of the wafer, was used for heating. The base pressure in the chamber was typically in the range of $<3 \times 10^{-10}$ Torr and rose to 2×10^{-9} Torr during heat cleaning. Following the heat cleaning, metal was deposited on the substrate. Titanium and zirconium layers were deposited by electron-gun evaporation, using a 3-kW e-gun. The UHV system used in this study has been described in more detail

elsewhere.[36] The Zr/Si samples were deposited with the substrates at room temperature and then annealed *in situ* to temperatures ranging from 500 °C to 950 °C, to cause the metal and silicon to react and form silicides. Anneal times varied from 15–20 min for $ZrSi_2$ films. The Ti/Si samples were prepared by deposition onto heated substrates with a deposition rate of 4 Å/s. The sample was held at the deposition temperature for 1 to 5 min after completion of the deposition. For both deposition methods, ramp-up and ramp-down rates were ~30 °C/min. LEED measurements were obtained after annealing to determine whether islanding had taken place. The sheet resistivity of thicker samples was measured with a four-point probe. The equipment consisted of a probe stage, a current source, and a voltage meter. The probe arrangement was linear, with the probe tips spaced 40 mils apart. The current used was 1 mA. The thicknesses of the samples, for the calculation of the resistivity from the measured resistance, were determined from the TEM cross-sectional micrographs.

Plan-view and cross-sectional TEM specimens were prepared from the wafers by prethinning followed by ion milling on a Gatan ion mill. The microscopy was performed on a JEOL 200CX and an Akashi 002B high resolution electron microscope. Cross-sectional TEM micrographs were used for measurements of the contact angles of the islands, and the surface and interface energies were calculated according to the solid-state capillarity model. Measurements of the contact angle were made with an ordinary protractor on prints and negatives of 30–40 islands of each material. The thicknesses and annealing temperatures of the samples were as follows: for $TiSi_2$, 50 and 100 Å of deposited Ti was annealed at 700–900 °C; for $ZrSi_2$, 50 and 100 Å of deposited Zr was annealed at 700–950 °C. The surface and interface energies were calculated for each island and then averaged over the entire sampling. The statistical validity of the values obtained was examined by a simple chi-squared test. An image capture system consisting mainly of a light table, CCD camera, Macintosh computer, and image analysis software was used to digitize the micrograph images so that calculations (e.g., the determination of faceting angles) could be done on them. Micrographs containing crossed (100) and (110) fringes in the silicon substrate were selected for analysis. The angles between the faceted planar region of interface and the Si(100) or Si(110) directions indicated by the fringes were measured using the "protractor" tool in the software.

IV. RESULTS

Before discussing the morphology of the films, we note the electrical properties of the $ZrSi_2$. The islanded films studied here were unsuitable for sheet resistivity measurements, but four-point probe measurements were performed on thicker $ZrSi_2$ (500–700 Å) films on Si(111) substrates. The results yielded values of 33–42 $\mu\Omega$-cm for the resistivity. These values are similar to those found by other investigators.[1,6,7,37] For comparison, the resistivity of $TiSi_2$ is 11–14 $\mu\Omega$-cm for the C54 phase and 55–65 $\mu\Omega$-cm for the C49 phase.[38] It may be questioned whether the difference in sheet resistivity of the C49 and C54 $TiSi_2$ is intrinsic to the different crystal structures or related to defects. We note that the sheet resistivity of the C49 $TiSi_2$ material is usually obtained from samples annealed to less than 750 °C. Higher temperature annealing could be beneficial for defect reduction. While it is possible to produce thin C49 $TiSi_2$ which is stable at high temperatures, these films tend to island, and sheet resistivity measurements become difficult.

A. Island formation and areal coverage

After the 50 or 100 Å of Ti deposition on Si(100) substrates, Auger spectroscopy showed Ti with no evidence of Si, and no LEED diffraction spots were observed. In contrast, after 700 °C and 800 °C UHV *in situ* anneals, respectively, a reconstructed LEED pattern was observed. The 2×1 pattern is characteristic of the reconstructed Si(100) surface, and this observation was interpreted as evidence that the film had begun to island, exposing the Si substrate.

In similar work, Jeon *et al.*[2] have reported that for 50–200 Å of Ti on Si(111) substrates, a 700 °C anneal is sufficient to produce a dim reconstructed 7×7 pattern. Here also, the observed diffraction was interpreted as the onset of island formation. We note that the results obtained here for samples prepared by deposition onto heated substrates were essentially the same as previous studies which involved room temperature deposition and *in situ* annealing.

In contrast, samples with 50–100 Å of Zr deposited on Si(111) surfaces and annealed to 700 °C showed no LEED pattern, only a diffuse brightness. A relatively strong 1×1 pattern plus weak 7×7 reconstructed spots were observed after an 800 °C anneal of Zr on Si(111), and a strong 7×7 pattern was observed only after a 900 °C anneal. For thicker samples (400–700 Å), even higher temperature anneals are required to produce even a weak 7×7 pattern. This indicates that the $ZrSi_2$ films are more resistant to islanding. The conclusion is confirmed by plan-view TEM. Figure 3 shows $TiSi_2$ films formed from 100 Å Ti on (a) Si(100) and (b) Si(111), well islanded following a 1 min anneal at 700 °C and 800 °C, respectively. Figure 4 shows $ZrSi_2$ films on Si(111) following a 700 °C, 15 min anneal, and a 950 °C, 15 min anneal. The films shown in Figs. 4(a) and 4(b) are formed from 100 Å

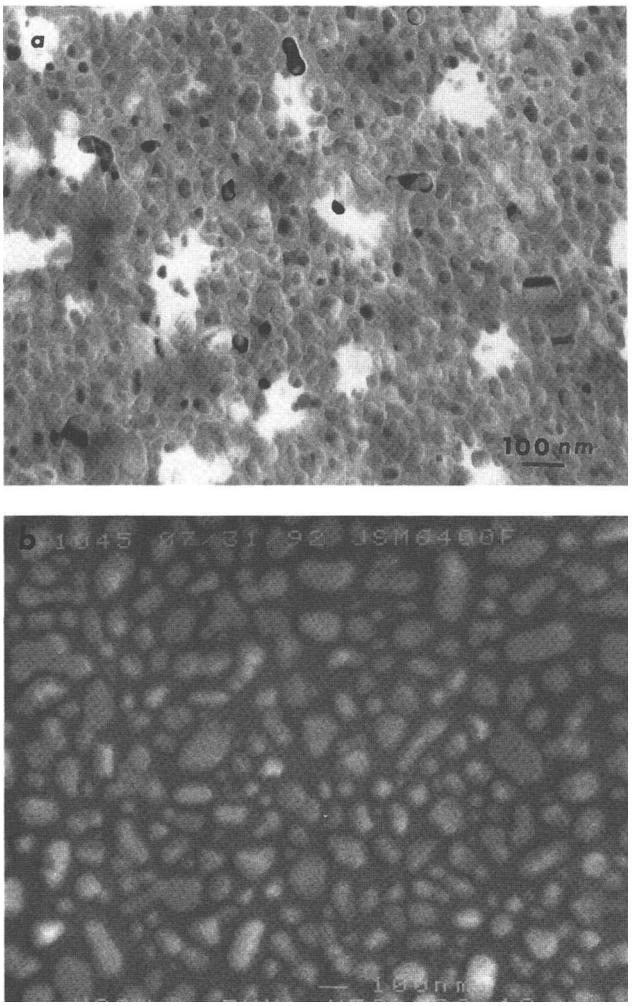

FIG. 3. The development of island morphology of $TiSi_2$ films: (a) plan-view TEM of a film formed from 100 Å Ti on Si(100) and annealed at 700 °C; (b) SEM of a film formed from 100 Å Ti on Si(111) and annealed at 800 °C.

of Zr. The film annealed at 700 °C is polycrystalline and appears to cover the substrate completely. The morphology is similar to that observed by Mu *et al.* for 300 Å Zr deposited at 2×10^{-6} Torr and RTA furnace annealed to 1100 °C.[27] The film annealed at 950 °C is still largely contiguous, although grains are observed that in some places have separated to expose the substrate, indicating the islanding process has begun.

Plan-view TEM and SEM were also used to determine the fraction of the substrate surface area covered by the films. The areal fraction (percentage of an area occupied by the silicide) was determined by overlaying a transparency with a grid on the print or negative, and comparing the number of points that fall on the phase with the total number of points to give a percentage.[39] By this technique, it was determined that for a sample with 100 Å of Ti on Si(100) annealed at 700 °C, in which the $TiSi_2$ film has islanded, the areal coverage is 60% [Fig. 3(a)]. For a $TiSi_2$ film on Si(111), formed from 100 Å of Ti and annealed at 800 °C, an areal coverage of 66% was obtained. In contrast, the $ZrSi_2$ film on Si(111) formed from 100 Å Zr and annealed at 700 °C was polycrystalline and covers the substrate completely, and only partial islanding was observed after a 950 °C anneal. A completely islanded $ZrSi_2$/Si(111) structure was, however, obtained from a 50 Å Zr/Si(111) sample after a series of three anneals at 700 °C, 850 °C, and 950 °C. This sample exhibited an areal coverage of 65%.

B. Contact angles and surface and interface energies

We use the contact angle measurements and Eq. (1) to determine the surface and interface energies of the films. Here we have used the reported values of the surface energies of the reconstructed (111) and (100) surfaces of Si.[40] Since contact angle measurements can obviously be made only on separated islands, islanded Ti/Si(100) films were obtained at 700, 800, and 900 °C for 100 Å Ti and at 800 and 900 °C for 50 Å Ti. The most islanded structures were observed and measured from the 900 °C anneal samples. We note that the $TiSi_2$ films on Si(100) should have the C54 structure. For Zr on Si(111), few islands were measured from the 850 °C anneal, and better statistics were observed after a 950 °C anneal. The results from the separate samples are summarized in Fig. 5.

The averages of all the measurements taken for each system are given in Table I. This table summarizes the surface and interface energies $TiSi_2$ on Si(100) and $ZrSi_2$ on Si(111) calculated from the contact angle measurements made in this study, with data from previous work on $TiSi_2$ on Si(111) included for comparison. Since in this study the surface and interface energies were determined for each measurement and then averaged, Table I does not contain any averaged angles, only averaged energies. A few extreme values were omitted from the averaging because they were believed to represent cases in which the appropriate measurement of the angles was ambiguous; for example, the edges of these islands were S-shaped rather than simple curves.

For the $TiSi_2$/Si(100) and $ZrSi_2$/Si(111) cases, the estimates of error given are the standard error from the statistical analysis. The standard deviations of the measurements were ~200 erg/cm^2 for all four surface and interface energies values. We note that it is possible to locate the central point of the distribution to better than a mean deviation. To further explore the statistical aspects of the data, histograms of the occurrences of surface or interface energies in a range were constructed. For each case the histograms exhibited a single peak, centered near the average value. The histograms of the data were fitted with a Gaussian distribution. An

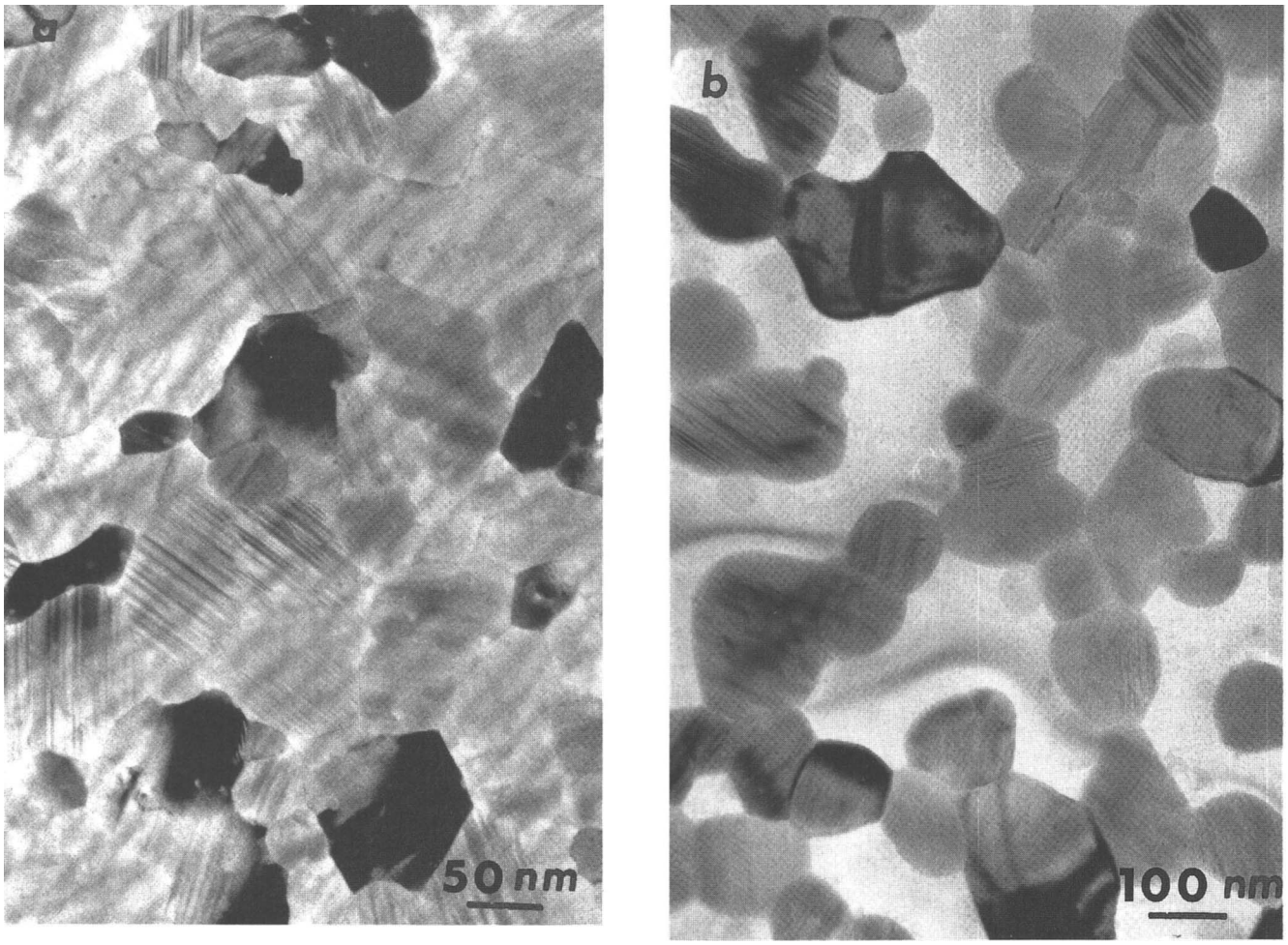

FIG. 4. Plan-view TEM showing the islanding process of $ZrSi_2$ on Si(111). In (a) the film has been subject to a 700 °C anneal and is polycrystalline; in (b) the film has been subject to a 950 °C anneal, and has begun to island, exposing the Si substrate. The films were formed from 100 Å Zr deposited on Si(111).

example is shown in Fig. 6. The results indicated that the distribution of individual values from which the averages were derived is more sharply peaked than Gaussian for the $ZrSi_2$ data, and indistinguishable from Gaussian for the $TiSi_2$ data. While the statistics do not allow either the statement that this is definitely a Gaussian distribution or that it is definitely not, we take assurance from these results that we are in general observing a single effect, namely the influence of surface and interface energies on island morphology.

We have also examined the variations in the distribution of data collected from the different sample structures and annealing temperatures. Since all the data taken together do not provide strong statistics, considerations of finer points within the data set are by nature speculative. Bearing this in mind, we proceed. A breakdown of the contributions of each sample to the surface and interface energy averages is given in Fig. 5. While no obvious trend is observed between the thickness of deposited metal and the surface and interface energies, we find an interesting trend corresponding to annealing temperature. The surface and interface energies tend to decrease for both cases. For Ti on Si(100), the interface energies show a substantial decrease with increasing annealing temperature, while the surface energy of the films remains relatively constant. This may indicate an increased alignment of the interface bonding or a tendency toward epitaxy.

C. Tendency to faceting

At each annealing temperature a certain percentage of the islands produced are observed to have faceted structure, and this percentage is observed to increase with increasing annealing temperature. In attempting to quantify the extent of the faceting of the various films, an island was counted as having "some faceted character" if it exhibited at least one faceted (flat) side, which was easily distinguished from the rounded droplet appearance of non-faceted islands. Several islands had more than

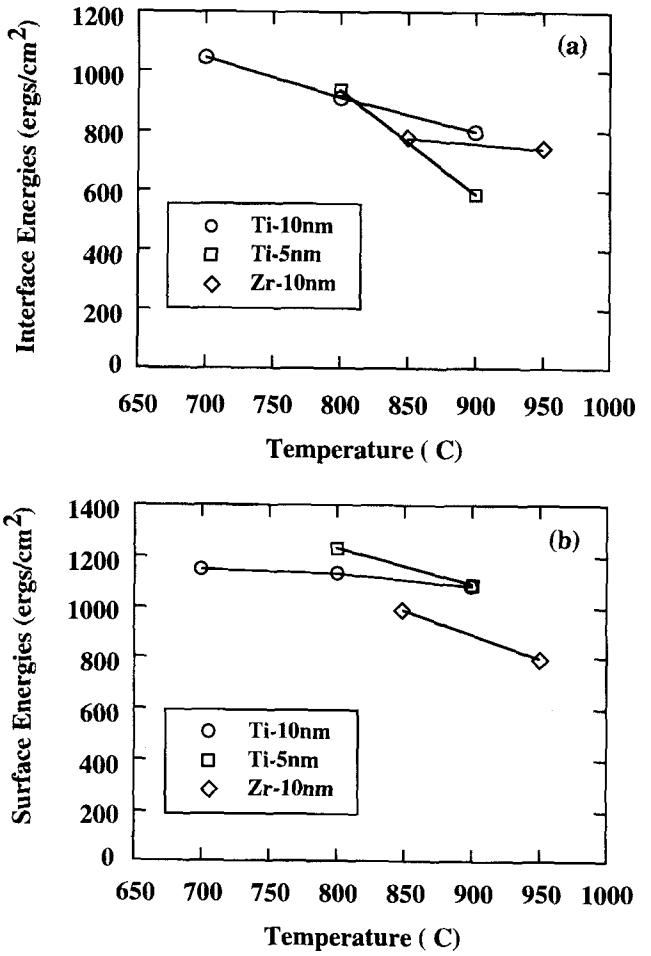

FIG. 5. The temperature dependence of the interface (a) and surface (b) energies deduced from the contact angle measurements.

one faceted side, and some had a completely faceted morphology. Figures 7 and 8 illustrate the progression of islanding observed by TEM cross section. Percentages of islands with faceted character were determined by counting the number of islands (in TEM cross sections) with "some faceted character" and comparing it with the total number of islands in the micrographs. The results are summarized in Fig. 9. Qualitatively, we observe that

TABLE I. Average surface and interface energies (in ergs/cm^2) for $TiSi_2$ and $ZrSi_2$ films on Si deduced from the contact angle measurements.

System	$\sigma_{Si^{40}}$	σ_{film}	$\sigma_{interface}$	$\sigma_{Si}/(\sigma_{film} + \sigma_{interface})$
$TiSi_2$/Si(100)	1210	1110 ± 160	860 ± 240	0.61
$ZrSi_2$/Si(111)	1019	940 ± 200	770 ± 220	0.60
$TiSi_2$/Si(111)	1019	780 ± 70	614 ± 50	0.73

The values represent averages over all temperatures, and the values for $TiSi_2$/Si(111) are from Ref. 2. The energy ratio in the last column is related to the areal coverage in the solid-state capillarity model.

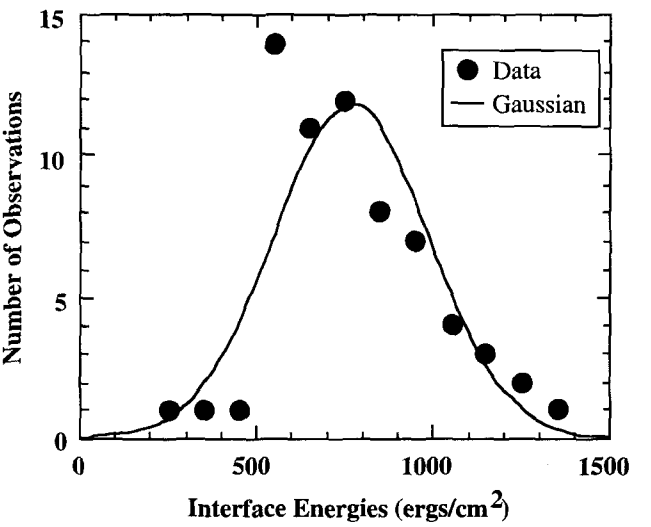

FIG. 6. Comparison of the distribution of interface energies of $ZrSi_2$ on Si(111) to a Gaussian distribution of the same mean and standard deviation.

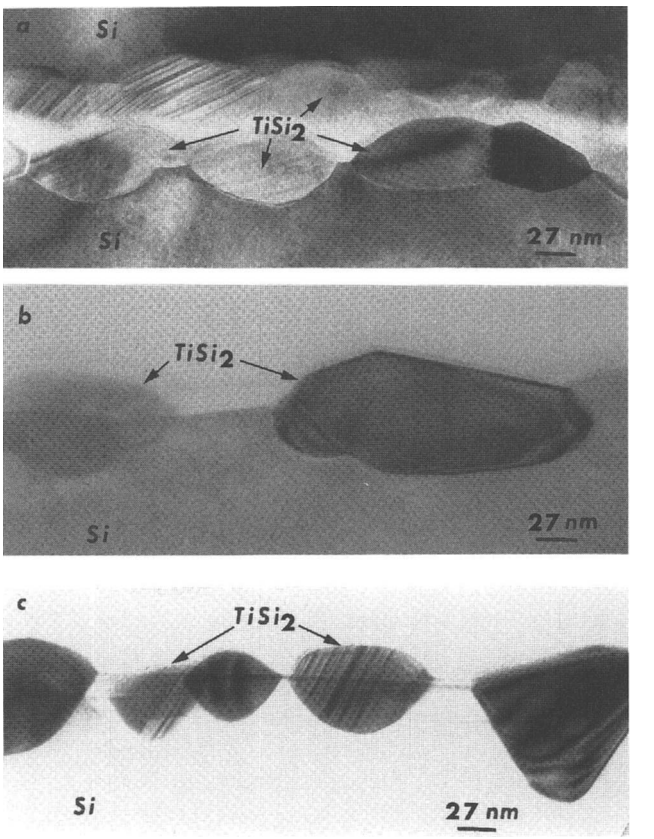

FIG. 7. Illustrating the progression of the faceted morphology for $TiSi_2$ on Si(100). The films were formed from 100 Å Ti on Si(100). The film in (a) was annealed at 700 °C and is moderately faceted, that in (b) was annealed at 800 °C and shows some islands with increased faceting, and that in (c) was annealed at 900 °C, and shows some more obviously faceted islands.

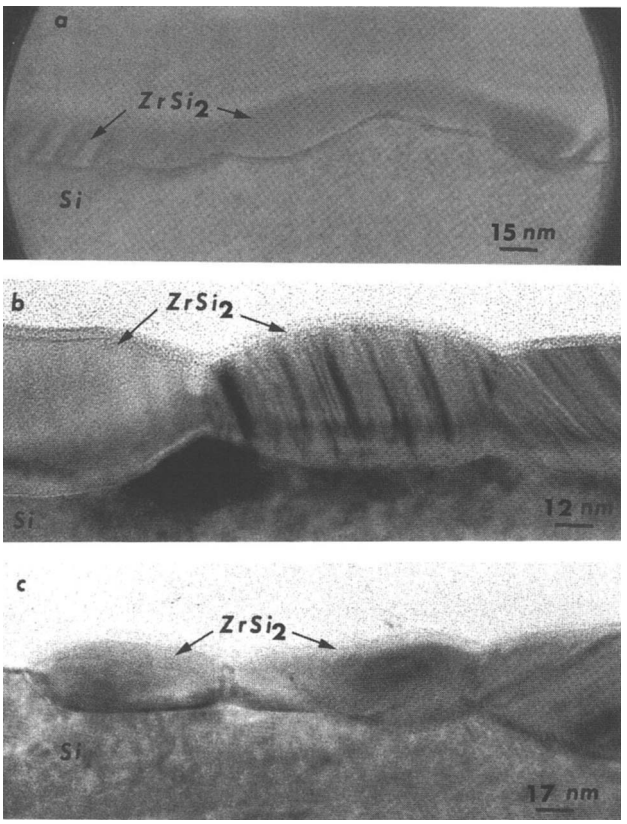

FIG. 8. Illustrating the progression of the faceted morphology for $ZrSi_2$ on Si(111). The film in (a) is formed from 100 Å Zr annealed at 700 °C and shows little if any faceted structure, that in (b) is formed from 100 Å Zr annealed at 800 °C and shows a small amount of faceting, mainly parallel to the interface (111), and the film in (c) is formed from 50 Å Zr subject to a 700 °C, 850 °C, and 950 °C anneal series, and shows stronger faceting along the (111) planes.

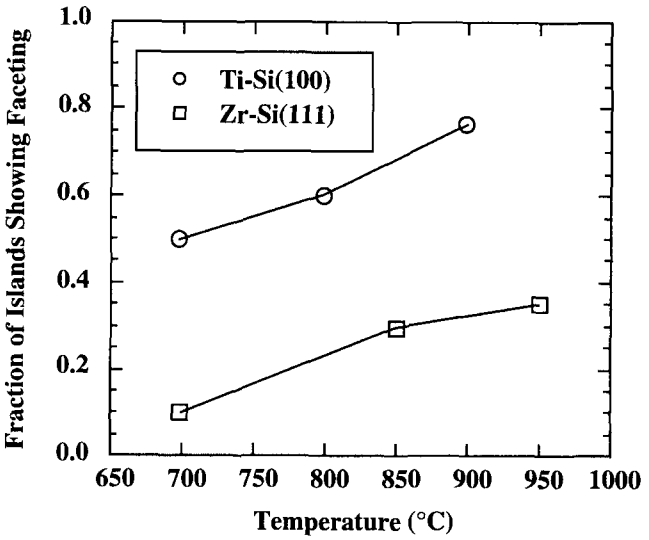

FIG. 9. The temperature dependence of the fraction of $TiSi_2$ or $ZrSi_2$ islands showing at least one faceted interface plane.

in $TiSi_2$ samples following a 900 °C anneal, the faceting of an island is generally more complete and more likely to include a faceted contact angle. In addition, the $ZrSi_2$ shows a substantially lower percentage of faceted islands.

Preliminary results of further experiments carried out in our laboratory on extremely thin silicide films at very high temperatures[41] show that the trend toward increased faceting continues. In particular, 7 Å thick $ZrSi_2$ films annealed at 900 and 1200 °C progress from mostly faceted to almost completely faceted morphologies, with a strong preference toward alignment with Si(110) type planes indicated by field-emission SEM data.

Analysis of the faceted structures to determine the existence of preferred planes was also performed on the cross-sectional HRTEM micrographs of the $TiSi_2$ and $ZrSi_2$. For $TiSi_2$ films on Si(100), the dominant faceting angles were measured to be 33–37° off the Si(100), and approximately parallel to the Si(100) plane. It should be noted that the precision that was possible using the "protractor" tool of the software was about ±3°. There were also small concentrations of measurements of angles in the ranges 55–64°, 75–79°, and 80–84° off Si(100). However, a few micrographs indicated that some of these more scattered measurements may actually be reflecting the presence of steps along the planes defined by the more dominant angles. Figure 10 shows one such micrograph. Here we can see that the apparent facets on both sides of the island are actually steps along a plane that was measured to be 34.5° off [100]. This is a ⟨211⟩ type direction, which is the trace of the intersection of the (111) and (110) planes. Therefore these steps represent faceting along Si(111) planes. The bottom of this island displays a few [100] steps. Both of these types of facets have also been observed by Catana *et al.*,[25,26] although the morphology of their Si(111) facets has a corrugated appearance, rather than the steps observed here.

Figure 11 shows the coexistence of different varieties of faceted $TiSi_2$ islands on Si(100). An example of an island with an extended (111) type facet (as well as some more complicated structures) is adjacent to a flat, (100)-faceted island.

An example of the faceting phenomenon for $ZrSi_2$ is given in Fig. 12. The figure shows $ZrSi_2$ islands with faceting parallel to the surface of the film, that is, apparently along (111) type planes. Steps along (111) planes are observed on other islands, similar to the steps on the $TiSi_2$ island in Fig. 10. The (111) faceting was the dominant type observed for $ZrSi_2$ islands on Si(111).

V. DISCUSSION

The first item to address from these results is the value of the sheet resistivity of the $ZrSi_2$ films. Given the many favorable properties that the material shares with

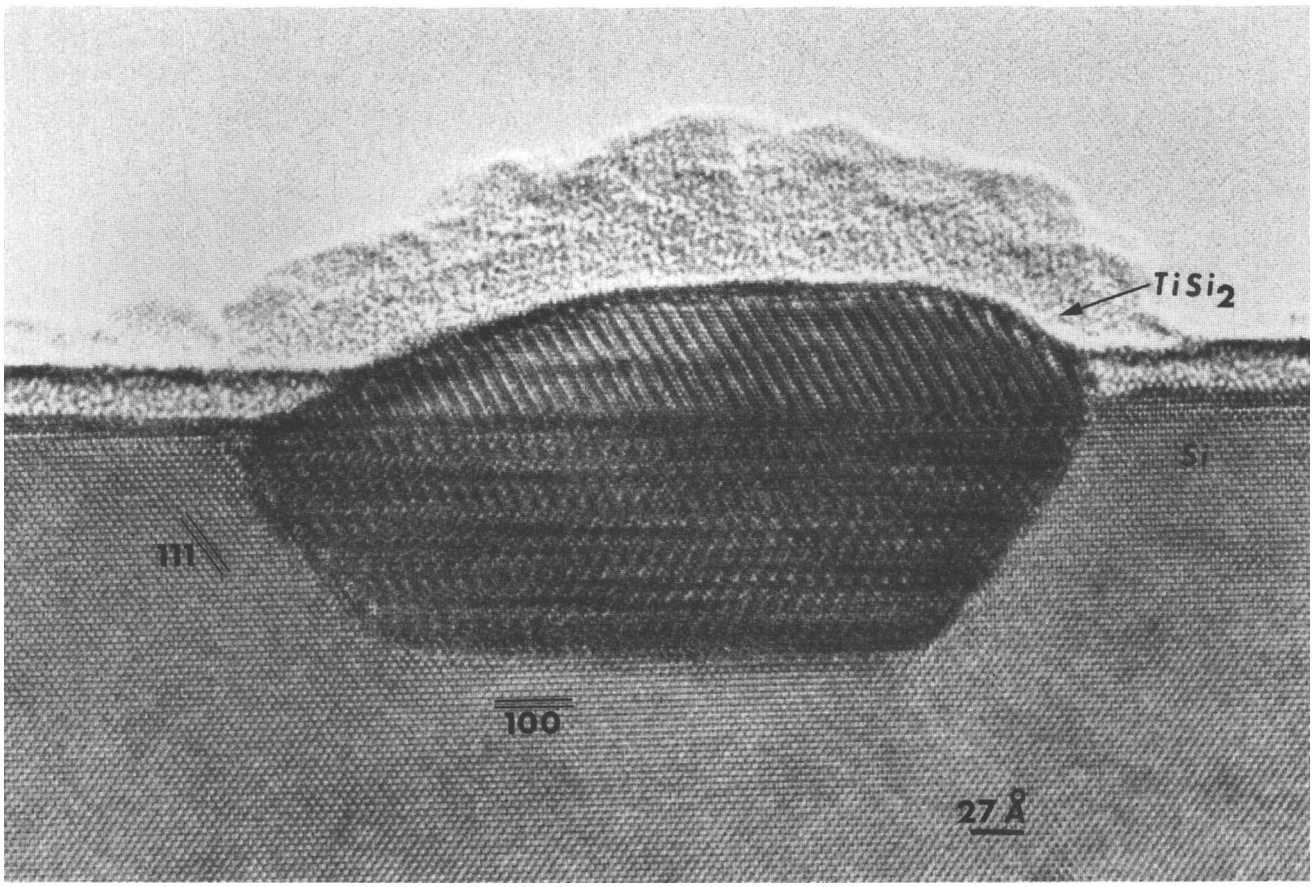

FIG. 10. HRTEM of a $TiSi_2$ island (100 Å Ti, 900 °C anneal) showing the stepped (111) and (100) morphologies.

$TiSi_2$, a sheet resistivity of 33–42 $\mu\Omega$-cm makes $ZrSi_2$ a potentially important silicide. In addition, applications of $ZrSi_2$ in alloy with $TiSi_2$ are being considered. As zirconium is an excellent getter (like titanium), care must be taken to avoid having impurities incorporated into the film during the growth process. We suggest that some of the previously reported higher sheet resistivities of $ZrSi_2$ are the result of impurities in the films. The samples discussed here were produced in UHV, to minimize the impurity problem.

The areal coverage and general island morphology are characteristics which are shown to be influenced by the surface and interface energies of the islands. We shall now examine the observed characteristics of the islands in relation to the measured energies of the films.

We have assumed that the 7 × 7 LEED pattern observed in these samples originates from the exposed substrate, and that this in turn is a sign that the film has islanded. A comparison of the LEED results for $TiSi_2$ and $ZrSi_2$ then indicates that $ZrSi_2$ begins to island at a considerably higher temperature than $TiSi_2$ on either Si(100) or Si(111), and the TEM measurements confirm this result. The tendency to islanding is essentially represented by the energy ratio $\sigma_{Si}/(\sigma_{film} + \sigma_{interface})$. When this term is 1.0 or greater, the system would be expected to exhibit uniform coverage. Thus, for values less than 1 islanding would occur, and the smaller the value, the larger the driving force for island formation. Thus, as indicated in Table I, the energy ratio of $ZrSi_2$ on Si(111) is comparable to that of $TiSi_2$ on Si(100), and both are lower than $TiSi_2$ on Si(111). Thus, the model would suggest that islanding of $ZrSi_2$ on Si(111) should occur at temperatures similar to those of $TiSi_2$ on Si(100) and at a lower temperature than $TiSi_2$ on Si(111). Since the initial temperature of island formation of $ZrSi_2$ on Si(111) is higher than that of $TiSi_2$ on both Si(111) and Si(100), we conclude that the surface energies are not the primary terms of this effect, and we suggest instead that kinetics play the main role. Zr and $ZrSi_2$ have higher melting points than Ti and $TiSi_2$, which suggests that they also have higher bond energies. Therefore, it is to be expected that a higher annealing temperature would be required to allow sufficient diffusion for completion of the islanding process.

The results pertaining to areal coverage are also related to the predictions of the solid-state capillarity model. The solid-state capillarity model predicts that the fraction of area covered by a film should also be proportional to the energy ratio $\sigma_{Si}/(\sigma_{film} + \sigma_{interface})$. Again, for islanded films, the more closely the ratio

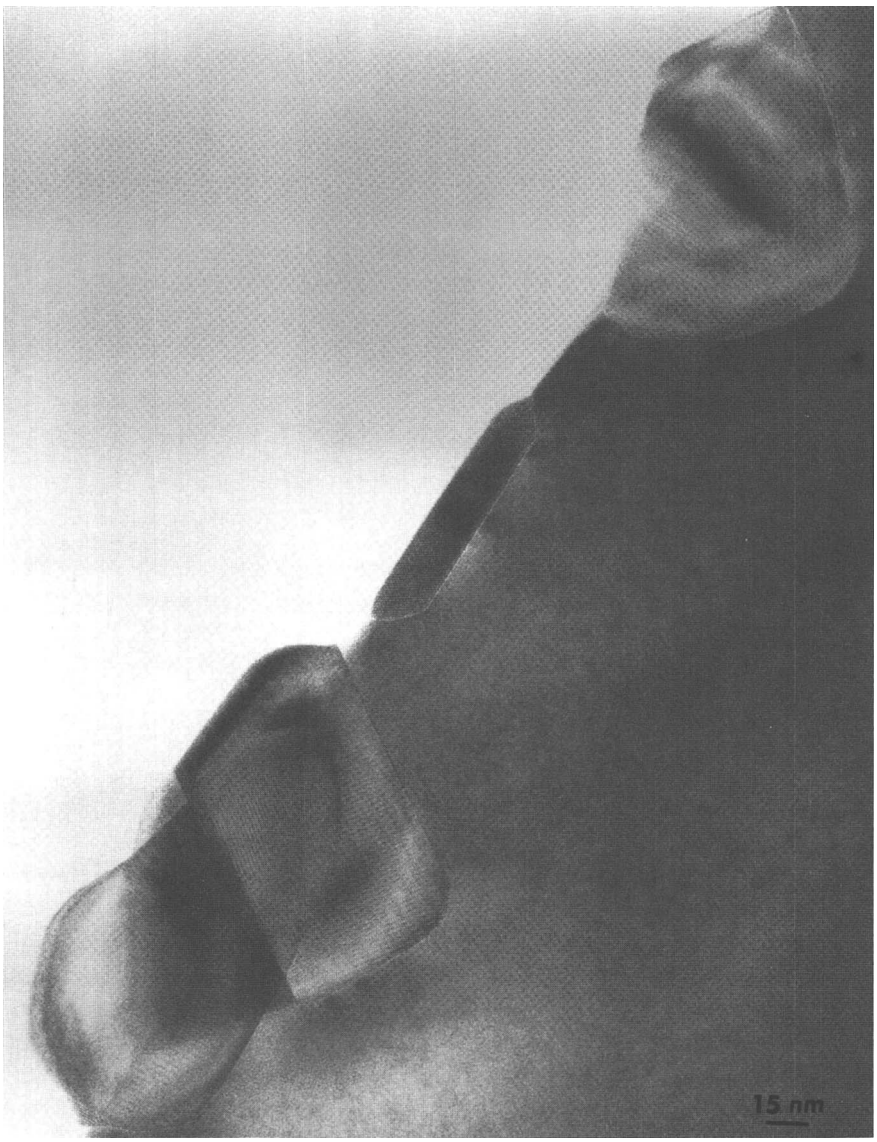

FIG. 11. Cross-sectional HRTEM of $TiSi_2$ islands showing a $TiSi_2$ island with an extended (111) type facet that is neighbor to a flat, (100) faceted island (100 Å Ti, 900 °C).

approaches one, the greater should be the areal coverage in a given system. Figure 13 plots the areal coverage for each of the three systems versus the energy ratio $\sigma_{Si}/(\sigma_{film} + \sigma_{interface})$. For Ti on Si(100) and (111), the results are consistent with the predicted trend. For $ZrSi_2$ on Si(111) the results are similar to the expected values, but they do not follow the same trend.

It is reasonable to question whether the measured contact angles represent an equilibrium structure or whether they represent a kinetically limited structure moving toward equilibrium. Probably the strongest argument to the validity of the measurements is that the contact angles show only modest variations with differences in annealing temperature (Fig. 5). We note that kinetic or diffusion processes generally exhibit an exponential behavior, and large changes for different annealing temperatures would be anticipated if the island structures were limited by diffusion. The picture that then develops is that when diffusion rates become substantial the films form island structures which reflect the surface and interface energies. In the experiments described here, the *in situ* LEED measurements are used to determine when and if the islanding has occurred. We note that while it is well established that the initial interdiffusion is dominated by the Si atoms, the island formation must also involve diffusion of the metal atoms.

As stated earlier, the solid-state capillarity model does not apply to islands with a faceted structure, and particularly those with a faceted contact angle. This fact can be used to help outline the regime in which the solid-state capillarity model applies. From the measurements of the percentage of faceted islands, it is clear that

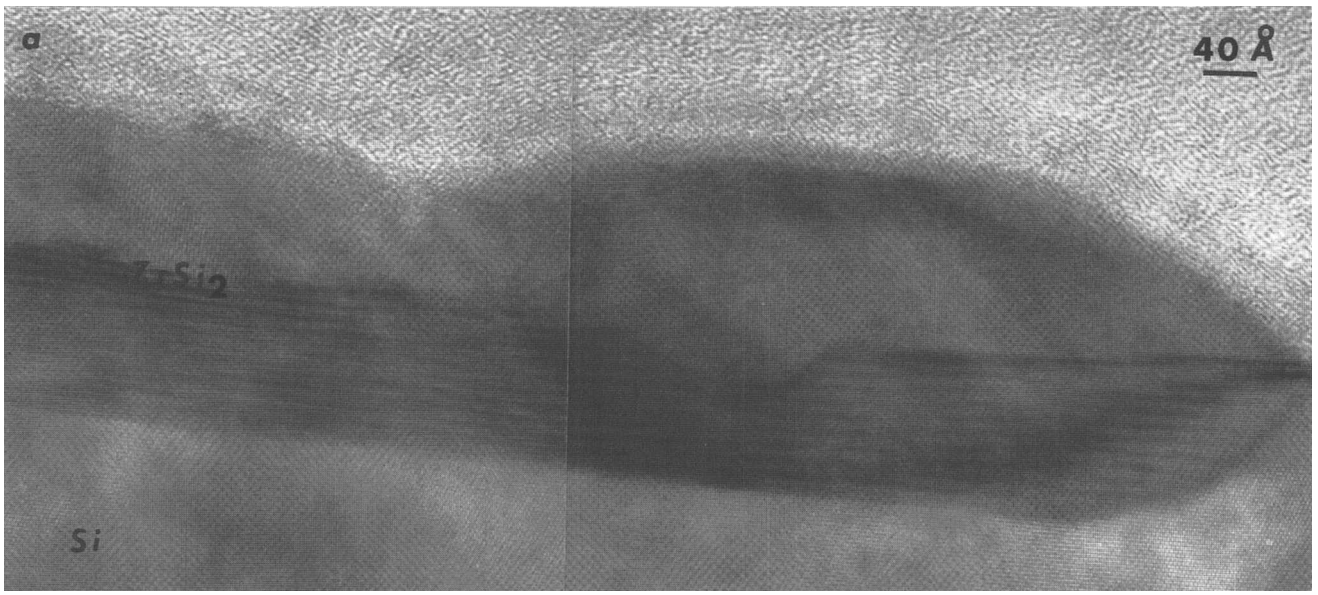

FIG. 12. Cross-sectional HRTEM of a $ZrSi_2$ island (50 Å Zr, 700 °C, 850 °C, and 950 °C anneals), showing an extended (111) interface.

this is not a sharp transition. There is first a range of annealing temperatures at which the islands formed are predominantly smoothly curved; the solid-state capillarity model applies to these. Then as the annealing temperature increases, the number of faceted islands gradually increases. Thus, in the presence of faceting, if surface-interface energy analysis is to be applied, it must take into account the differing energies of the crystallographic planes along which faceting occurs. The results shown here indicate that faceting begins at lower temperatures in $TiSi_2$ than in $ZrSi_2$. Preliminary results on the $ZrSi_2$ films formed with 7 Å deposited Zr show

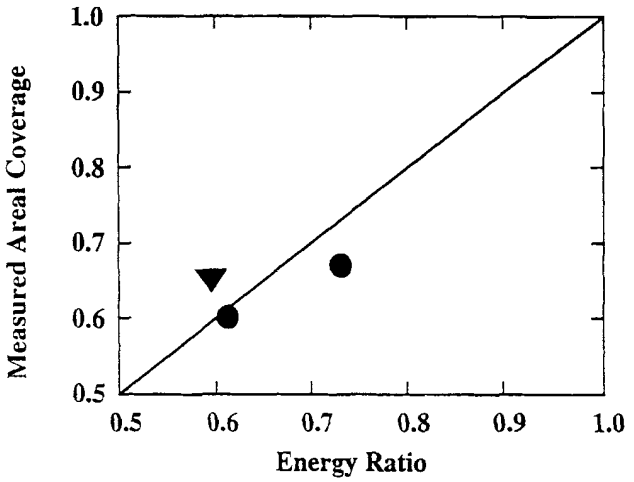

FIG. 13. Relation of measured areal and the energy ratio $\{\sigma_{Si}/(\sigma_{film} + \sigma_{interface})\}$ related to the surface coverage from the solid-state capillarity model. The triangle represents the $ZrSi_2$/Si(111), and the circles are the $TiSi_2$ on Si(100) and (111). The solid line indicates the expected relation and is not a fit to the data.

that after high temperature annealing (>1100 °C), the faceting process goes to completion.[41]

We suggest that the reason for the faceting is that once an initial equilibrium has been reached by minimization of the appropriate surface area and other general surface energy considerations, the thermal energy supplied by a high-temperature anneal allows the island to be driven toward another equilibrium by orienting along the lowest-energy planes, particularly at the interface. This process may involve nucleation and hence exhibit a nucleation barrier. The preference of low energy planes is supported by the preponderance of faceting observed along Si(111) and Si(100) planes for $TiSi_2$ and along Si(111) planes for $ZrSi_2$ (although others may appear upon higher temperature annealing). We note that several epitaxial relationships have been reported in the literature, involving C54 $TiSi_2$ and (111) type planes of silicon,[26,42] as well as some involving C49 $TiSi_2$ and (111)[3] and (100)[43] type planes of silicon, and $ZrSi_2$ and (111) type planes of silicon. By the criteria generally used to define epitaxy (that is, an overlayer grown in a specific crystallographic orientation relation to the substrate), many of the films in this study also contain regions of epitaxial growth, which are, of course, low-energy surfaces.

In the case of $TiSi_2$, one reason for both the increase in faceted islands and the apparent change in interface energy with annealing temperature may be the transition from C49 to C54 phase. Recall that for 100 Å of Ti deposited on Si(100), the transition occurs somewhere between 700 and 800 °C. It has been proposed that the two structurally different phases of $TiSi_2$ have different surface and interface energies, due to the different possible orientation relationships with the substrate. This

could account for the difference in interface energies between samples annealed at 700 °C and 800 °C. There are different epitaxial relations reported between C54 $TiSi_2$ and silicon and between C49 $TiSi_2$ and silicon, and since an epitaxial interface is likely a low energy surface, an island once oriented would stay oriented. Thus, if faceting or stepping affects the contact angle and interface-substrate angle of several islands, the calculated surface and interface energy averages would also be affected.

VI. SUMMARY

The surface and interface energies of $ZrSi_2$ on Si(111) have been calculated according to a solid-state capillarity model, and compared to those of $TiSi_2$ on Si(111) and (100). The fact that $TiSi_2$ on Si(111) has lower surface and interface energies than $ZrSi_2$, while $TiSi_2$ on Si(100) has higher surface and interface energies than $ZrSi_2$, runs counter to the expectations of the model (which are based on observations of islanding temperature). This indicates that kinetic effects must be considered along with the energy considerations of the model. The results regarding areal coverage agree generally with the predictions of the model, essentially that films with lower surface and interface energies should show greater areal coverages.

An understanding of the interface structure involved in forming the different morphologies was obtained by HRTEM. Both $ZrSi_2$ and $TiSi_2$ showed faceting along Si(111) type planes, with some extended, smooth morphologies and some stepped structures, and apparent epitaxial relation to the substrate. $TiSi_2$ also showed faceting along Si(100) type planes. It was noted that the $TiSi_2$ samples were more extensively faceted, and it is speculated that $ZrSi_2$ may show other faceting planes on Si(100) substrates or when subject to higher temperature anneals. The faceted structure was suggested to be a continuation of the progression toward lower energy situations. The existence of a majority of islands in a highly faceted morphology was noted as a case in which the solid-state capillarity model would no longer apply.

ACKNOWLEDGMENTS

We gratefully acknowledge the assistance of Professor D. Maher in the TEM measurements and analysis. We also acknowledge the assistance and helpful discussions of David Aldrich, Y.L. Chen, Ann Edwards, and Yuan Dao. This study was supported in part by the National Science Foundation through Grant DMR-9204285.

REFERENCES

1. S.P. Murarka, J. Vac. Sci. Technol. **17**, 775 (1980).
2. H. Jeon, C.A. Sukow, J.W. Honeycutt, G.A. Rozgonyi, and R.J. Nemanich, J. Appl. Phys. **71**, 4269 (1992).
3. H. Jeon, C.A. Sukow, J.W. Honeycutt, T.P. Humphreys, G.A. Rozgonyi, and R.J. Nemanich (Mater. Res. Soc. Symp. Proc. **181**, Pittsburgh, PA, 1990), p. 595.
4. I. Engström and B. Loennberg, J. Appl. Phys. **63**, 4476 (1988).
5. W.B. Pearson, *The Crystal Chemistry and Physics of Metals and Alloys* (John Wiley-Interscience, New York, 1972).
6. K. Pomoni and J. Salmi, J. Phys. D (Appl. Phys.) **24**, 727 (1991).
7. M. Setton and J.v.d. Speigel, J. Appl. Phys. **70**, 193 (1991).
8. K. Holloway and R. Sinclair, J. Appl. Phys. **61**, 1359 (1987).
9. R. Beyers and R. Sinclair, J. Appl. Phys. **57**, 5240 (1985).
10. R. Butz, G.W. Rubloff, T.Y. Tan, and P.S. Ho, Phys. Rev. B **30**, 5421 (1984).
11. I.J.M. Raaijmakers, A.H. Reader, and P.H. Oosting, J. Appl. Phys. **63**, 2790 (1988).
12. X. Wallart, J.P. Nys, and G. Dalmai, Appl. Surf. Sci. **38**, 49 (1989).
13. H.J.W. van Houtum, I.J.M.M. Raaijmakers, and T.J.M. Menting, J. Appl. Phys. **61**, 4269 (1987).
14. T. Yamauchi, S. Zaima, K. Mizuno, H. Kitamura, Y. Koide, and Y. Yasuda, Appl. Phys. Lett. **57**, 1105 (1990).
15. H.C. Cheng and L.J. Chen, Appl. Phys. Lett. **46**, 562 (1985).
16. J.Y. Cheng and L.J. Chen, J. Appl. Phys. **68**, 4002 (1990).
17. T. Yamauchi, S. Zaima, K. Mizuno, H. Kitamura, Y. Koide, and Y. Yasuda, J. Appl. Phys. **69**, 7050 (1991).
18. C.A. Sukow, M.S. Thesis, North Carolina State University (1992).
19. P. Revesz, L.R. Zheng, L.S. Hung, and J.W. Mayer, Appl. Phys. Lett. **48**, 1591 (1986).
20. A. Gupta, G.A. West, and K.W. Beeson, J. Appl. Phys. **58**, 3573 (1985).
21. R. Burmester, H. Joswig, and A. Mitwalsky, in *19th European Solid State Device Research Conference,* edited by A. Heuberger, H. Ryssel, and P. Lange (Springer-Verlag, Berlin, 1989), p. 233.
22. Y. Omura, H. Inokawa, and K. Izumi, J. Mater. Res. **6**, 1238 (1991).
23. H. Kuwano, J.R. Phillips, and J.W. Mayer, Appl. Phys. Lett. **56**, 440 (1990).
24. L.J. Chen, I.W. Wu, J.J. Chu, and C.W. Nieh, J. Appl. Phys. **63**, 2778 (1988).
25. A. Catana, M. Heintze, F. Lévy, P.E. Schmid, and P. Stadelmann, *Semiconductor Silicon,* edited by G.C. Harbeke and M.J. Schults (Springer Series in Materials Science, Berlin, 1989), Vol. 13, p. 276.
26. A. Catana, P.E. Schmid, M. Heintze, and F. Lévy, J. Appl. Phys. **67**, 1820 (1990).
27. S. Mu, J. Lue, and I. Wu, J. Phys. Chem. Solids **49**, 1389 (1988).
28. A. Bourret, F.M. d'Heurle, F.K. LeGoues, and A. Charai, J. Appl. Phys. **67**, 241 (1990).
29. A.P. Botha and R. Pretorius, in *Thin Films and Interfaces,* edited by P.S. Ho and K.N. Tu (Mater. Res. Soc. Symp. Proc. **10**, North Holland, Amsterdam, 1982), p. 129.
30. H. Jeon and R.J. Nemanich, Thin Solid Films **184**, 357 (1990).
31. R.J. Nemanich, R. Fiordalice, and H. Jeon, IEEE J. Quant. Elect. **25**, 997 (1989).
32. T.P. Nolan, R. Sinclair, and R. Beyers, J. Appl. Phys. **71**, 720 (1992).
33. F.M. d'Heurle, J. Mater. Res. **3**, 167 (1988).
34. J.J. Chu, I.C. Wu, and L.J. Chen, J. Appl. Phys. **61**, 549 (1987).
35. N.K. Adam, *The Physics and Chemistry of Surfaces* (Dover, New York, 1968).
36. H. Jeon, Thesis, North Carolina State University (1990).
37. Y. Igarashi, T. Yamaji, S. Nishikawa, and S. Ohno, Appl. Surf. Sci. **41–42**, 282 (1989).
38. C.A. Pico and M.G. Lagally, J. Appl. Phys. **64**, 4957 (1988).

39. J. C. Russ, *Computer-Assisted Microscopy: The Measurement and Analysis of Images* (Plenum, New York, 1990).
40. T. Takai, T. Halicioglu, and W. A. Tiller, Surf. Sci. **104**, 341 (1985).
41. B. L. Kropman, C. A. Sukow, and R. J. Nemanich, in *Evolution of Surface and Thin Film Microstructure*, edited by H. A. Atwater, E. H. Chason, M. L. Grabow, and M. G. Lagally (Mater. Res. Soc. Symp. Proc. **280**, Pittsburgh, PA, 1993), pp. 589–592.
42. K. H. Kim, J. L. Jeoung, D. J. Seo, C. K. Choi, S. R. Hong, D. K. Jeoung, S. C. Kim, J. Y. Lee, and M. A. Nicolet, J. Appl. Phys. **71**, 3812 (1992).
43. M. S. Fung, H. C. Cheng, and L. J. Chen, Appl. Phys. Lett. **47**, 1312 (1985).